Focal Spot Blur Reduction by Deconvolution on CT Projections

Lucas Determan[1*], Kirk Busche[1], Pradeep Bhattad[1]
*ldeterman@4nsi.com
[1]North Star Imaging, Inc., Rogers, MN, USA

Introduction

High-energy X-ray sources typically generate X-rays from a larger focal spot. This enables the imaging of dense objects but can lead to reduced image quality due to increased geometric unsharpness. This paper investigates and compares computational methods for reducing the resulting blur. Two approaches for acquiring the focal spot blur intensity profile are explored, as well as the subsequent removal of the induced blur in the CT projections via deconvolution. The modified CT projections are reconstructed using standard filtered backprojection (FBP) to assess the blur reduction performance. The results of the deconvolution approaches are evaluated both in 2D (projection) space and in 3D (reconstruction) space using spatial resolution, contrast-to-noise, and qualitative analyses.

Methods

1. Recover the blur model

X-ray imaging can be formulated as a convolution process

$$\boldsymbol{y} = \boldsymbol{k} * \boldsymbol{x} + \boldsymbol{n}$$

where $\boldsymbol{k}$ is the focal spot blurring kernel, $\boldsymbol{x}$ is the unknown sharp image, $\boldsymbol{y}$ is the measured blurred image, and $\boldsymbol{n}$ is the observed noise. Solving the inverse is recovering the sharp image using a known blurring kernel. To recover the blurring kernel, methods for measuring the focal spot using an image of an ASTM plaque-type Image Quality Indicator (IQI) hole were investigated. Two methods explored for kernel recovery include a radial filtered backprojection (FBP) technique [2][3][4] and an iterative blind deconvolution technique (IBD) [5]. The plaque-type IQI functioned as a circular straight edge allowing for both methods to operate on it and recover a blur model.

2. Deconvolve the radiographs & reconstruct CT scan

Two methods were investigated for applying deconvolution or estimating the unknown sharp image $\boldsymbol{x}$. The first is a direct inverse filtering technique: regularized Wiener deconvolution [6]. It provides a fast method however it is susceptible to artifacts such as ringing and careful choice of the regularization factor. To address some of these shortcomings, a constrained iterative deconvolution technique—conjugate gradient deconvolution (CGD)—was used [5]. Each technique was used and evaluated by applying it to the radiographs acquired for a circular CT scan.

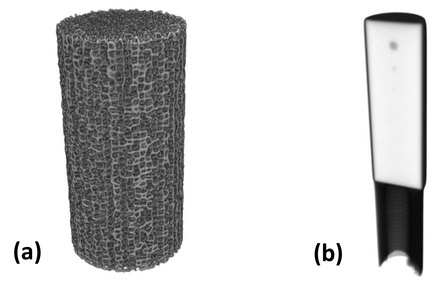

Figure 1: (a) Additively manufactured (AM) lattice part and (b) AM cylinder with various sized voids.

Experiment & Results

Two high energy systems were used, including a North Star Imaging (NSI) X5000 with a 450 kV source and a NSI MeVX with a 9 MeV source. Blur models were recovered for both using the two different techniques for recovery and were acquired before a circular CT scan was conducted. Then, using the acquired CT scan, the two different methods of deconvolution were applied to the radiographs and later reconstructed. The parts considered were an AM lattice and AM cylinder where the cylinder was used for ASTM E1695 spatial resolution and contrast to noise 3D reconstruction analysis. Images of a line pair gauge were also acquired to measure the performance on the 2D radiographs.

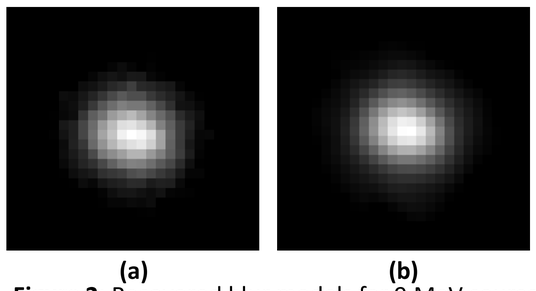

Figure 2: Recovered blur models for 9 MeV source **(a)** radial FBP & **(b)** IBD.

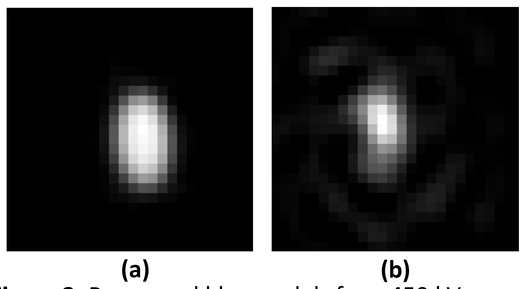

Figure 3: Recovered blur models for a 450 kV source **(a)** radial FBP & **(b)** IBD.

Figure 4a: Acquired 450 kV IQI hole image with no post processing.

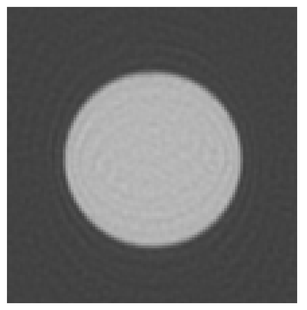

Figure 4b: Blur model recovered using radial FBP, deconvolved using Wiener filtering.

Figure 4c: Blur model recovered using IBD, deconvolved using Wiener filtering.

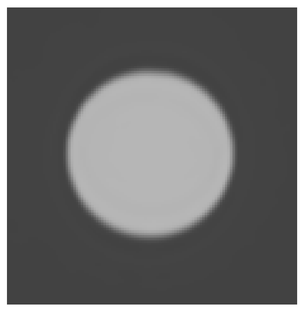

Figure 4d: Blur model recovered using radial FBP, deconvolved using CGD.

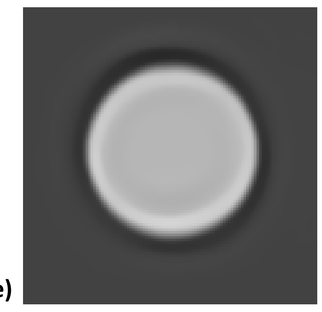

Figure 4e: Blur model recovered using IBD, deconvolved using CGD.

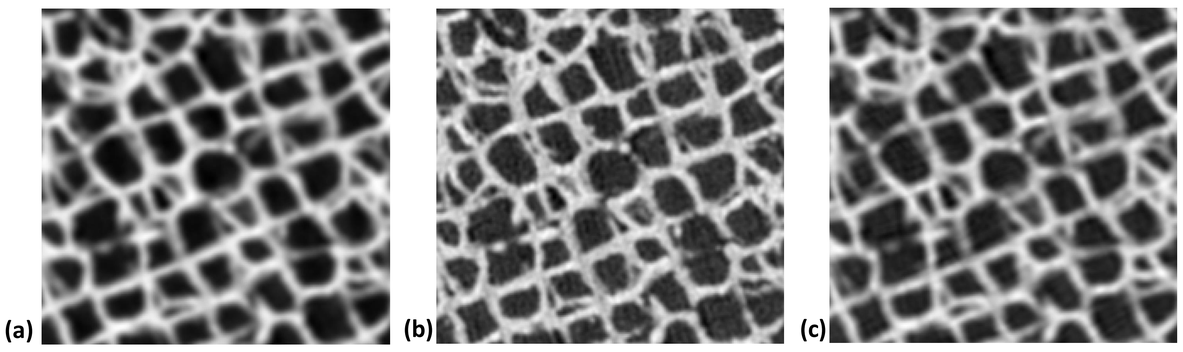

Figure 5: A CT slice of the additively manufactured (AM) lattice part where **(a)** baseline no deconvolution reconstruction, **(b)** Wiener deconvolution, and **(c)** conjugate gradient deconvolution.

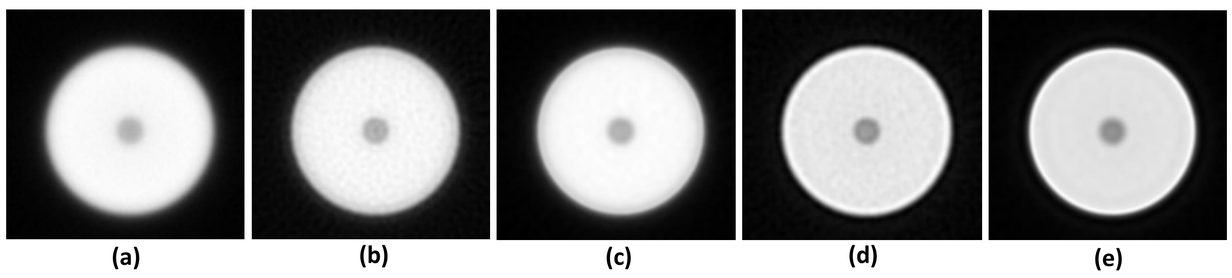

Figure 6: A CT slice of the additively manufactured (AM) cylinder part where **(a)** baseline no deconvolution reconstruction, **(b)** radial FBP with Wiener deconvolution, **(c)** radial FBP with CGD, **(d)** IBD recovery with Wiener deconvolution, and **(e)** IBD recovery with CGD.

Technique	SRb 2D Line Pair Gauge	SRb ASTM E1695	CNR ASTM E1695
Baseline	338.6 µm	359 µm	201.61
Radial FBP w Wiener Filter	147.6 µm	272.2 µm	94.7
Radial FBP w CGD	285.2 µm	169.6 µm	250.72
IBD w Wiener Filter	157.7 µm	274 µm	92.66
IBD w CGD	285 µm	178 µm	234.81

Table 1: 9 MeV results for 2D and 3D analysis of the spatial resolution and contrast to noise.

Discussion & Conclusion

Obtaining an accurate model of the focal spot blur which can be properly applied to a CT scan's acquired projections is not trivial. Changes to shape, size, or intensity of the blur significantly impact the performance of the deconvolution procedure. Methods for blur model recovery are highly dependent on proper alignment to minimize parallax blur. Deconvolution is highly sensitive to small perturbations like noise, both in the blur model and the projection data. Direct inverse filtering is insufficient for real-world applications without additional processing. Discrepancies between the 2D and 3D analysis are attributed to the CGD volumes consisting of more ringing artifact and a lack of robustness in ASTM E1695 spatial resolution analysis.

Overall, the results show that applying the blur model improved the spatial resolution of the resulting projections. Doing this with minimal artifacts depends on the techniques used throughout the procedure. Noise was a significant factor in recovering the CT projection effectively, showing that improvement in spatial resolution can be outweighed by impact of the noise.

References

[1] A. Levin, Y. Weiss, F. Durand and W. T. Freeman, "Understand and evaluating blind deconvolution algorithms," IEEE Conference on Computer Vision and Pattern Recognition, pp. 1964-1971, 2009.
[2] T. S. Cho, S. Paris, B. K. P. Horn and W. T. Freeman, "Blur Kernel Estimation using the Radon Transform," CVPR, pp. 241-248, 2011.
[3] B. A. Bircher, F. Meli, A. Kung and A. Sofiienko, "Traceable x-ray focal spot reconstruction by circular edge analysis: from sub-microfocus to mesofocus," Measurement Science and Technology, vol. 33, no. 074005, 2022.
[4] G. Di Domenico, P. Cardarelli, A. Contillo, A. Taibi and M. Gambaccini, "X-ray focal spot reconstruction by circular penumbra analysis—Application to digital radiography systems," Medical physics, vol. 43, p. 294–302, 2016.
[5] A. Levin, Y. Weiss, F. Durand and W. T. Freeman, "Efficient Marginal Likelihood Optimization in Blind Deconvolution," CVPR 2011, pp. 2657-2664, 2011.
[6] N. Wiener, Extrapolation, interpolation, and smoothing of stationary time series: with engineering applications, The MIT press, 1949.
[7] W. H. Richardson, "Bayesian-based iterative method of image restoration," JoSA, vol. 62, p. 55–59, 1972.
[8] ASTM E1165 - 12 (Reapproved 2017), Standard Test Method for Measurement of Focal Spots of Industrial X-Ray Tubes by Pinhole Imaging, West Conshohocken, PA: ASTM International, 2017.
[9] ASTM E1695 - 20e1, Standard Test Method for Measurement of Computed Tomography (CT) System Performance, West Conshohocken: ASTM International, 2020.
[10] ASTM E2002 - 15, Standard Practice for Determining Total Image Unsharpness and Basic Spatial Resolution in Radiography and Radioscopy, West Conshohocken: ASTM International, 2015.